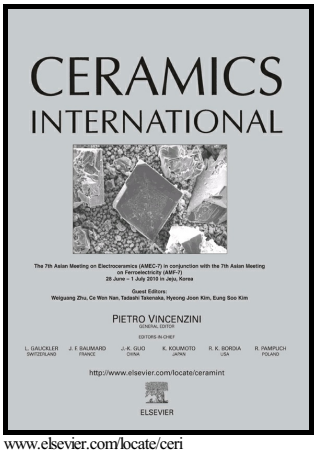

www.elsevier.com/locate/ceri

Characteristics of $Ba(Zr_{0.1}Ce_{0.7}Y_{0.2})O_{3-\delta}$ Nano-powders Synthesized by Different Wet-chemical Methods for Solid Oxide Fuel Cells

Sung Hwan Min, Jin Goo Lee, Ok Sung Jeon, Myeong Geun Park, Kwang Hyun Ryu, Jae-ha Myung, Yong-Gun Shul

PII: S0272-8842(17)32124-7
DOI: http://dx.doi.org/10.1016/j.ceramint.2017.09.195
Reference: CERI16366

To appear in: *Ceramics International*

Received date: 6 September 2017
Revised date: 20 September 2017
Accepted date: 24 September 2017

Cite this article as: Sung Hwan Min, Jin Goo Lee, Ok Sung Jeon, Myeong Geun Park, Kwang Hyun Ryu, Jae-ha Myung and Yong-Gun Shul, Characteristics of $Ba(Zr_{0.1}Ce_{0.7}Y_{0.2})O_{3-\delta}$ Nano-powders Synthesized by Different Wet-chemical Methods for Solid Oxide Fuel Cells, *Ceramics International,* http://dx.doi.org/10.1016/j.ceramint.2017.09.195

Characteristics of $Ba(Zr_{0.1}Ce_{0.7}Y_{0.2})O_{3-\delta}$ Nano-powders Synthesized by Different Wet-chemical Methods for Solid Oxide Fuel Cells

Sung Hwan Min,[a†] Jin Goo Lee,[b†] Ok Sung Jeon,[a] Myeong Geun Park,[a] Kwang Hyun Ryu[c], Jae-ha Myung,[d] and Yong-Gun Shul[a,b*]

[a]Department of Chemical and Biomolecular Engineering, Yonsei University, Seoul 120-749, Republic of Korea

[b]School of Chemistry, University of St Andrews, St Andrews, Fife, KY16 9ST, UK

[c]LTC Co., Ltd., Seoul 120-749, Anyang, Gyeonggi, Republic of Korea

[d]Conversion Materials Laboratory, Korea Institute of Energy Research, 152 Gajeong-ro, Yuseong-gu, Daejeon, 34129, Republic of Korea

Abstract

$Ba(Zr_{0.1}Ce_{0.7}Y_{0.2})O_{3-\delta}$ nano-particles were prepared by different wet-chemical synthesis, Pechini (BZCY(P)) and co-precipitation (BZCY(C)), respectively. The BZCY(C) powders have a particle size in range of about 50~150 nm, which is smaller than the BZCY(P) powders with about 500~900 nm. Both the BZCY materials show perovskite structures, but there are impurities in the BZCY (P). Moreover, the electrolyte density was higher in the BZCY (C) than the BZCY (P). The single cells with BZCY (C) electrolytes exhibited about 0.23 W cm^{-2} at 600 °C and about 0.31 W cm^{-2} at the same temperature were obtained when the anode-functional layer was introduced between the anode and electrolyte. Thus, the BZCY prepared by carbonate-derived co-precipitation method can be more favorable for high-purity and dense electrolytes in the solid oxide fuel cells than the BZCY prepared by Pechini method.

Keywords: solid oxide fuel cell, BZCY, functional layer, nickel penetration, proton conductor

*Corresponding author. Tel: +82 2 2123 2758; fax: +82 2 312 6507; e-mail : shulyg@yonsei.ac.kr (Y.G. Shul).

1. Introduction

Solid oxide fuel cells (SOFCs) have attracted much attention worldwide as a stationary power generation system due to their high-energy efficiency and low environmental impact [1-4]. However, the high operating temperature (800~1000 ^{o}C) leads to increase in maintenance cost and system degradation [5]. One approach to lowering the SOFCs operation temperature is to use proton conductors instead of the conventional oxygen-ion conductors as an electrolyte material because of their high ionic conductivities and low activation energy for proton conduction [6-10].

Iwahara et al. reported that several perovskite-type oxides such as $BaCeO_3$, $SrCeO_3$, $SrZrO_3$ and $BaZrO_3$ show a good proton conductivity of 10^{-2}~ 10^{-3} Scm^{-1} at a temperature range of 600~ 1000 ^{o}C [11-13]. However, the $BaCeO_3$ and $SrCeO_3$ have poor chemical stability in acidic gases such as CO_2 and SO_2 or moisture [7, 14]. The $SrZrO_3$ and $BaZrO_3$ have excellent chemical stability, but their poor sintering properties require high energy consumption for the dense electrolytes [15]. Recently, Zuo et al. reported that $Ba(Zr_{0.1}Ce_{0.7}Y_{0.2})O_{3-\delta}$ (BZCY) shows a fast-protonic conductivity and enhanced chemical and thermal stability over a wide range of operating conditions [16].

There have been many preparation methods for BZCY nano-powders such as modified citrate method and modified co-pressing method.[17,18] Zhiwen et al reported the uniform fine NiO–BZCY composite powders were prepared by co-synthesis method, and the membrane thickness was about 30 μm. However, after two-step sintering in air and 5%H_2/Ar, a dense and crack-free Ni–BZCY asymmetric membrane was obtained with a thickness of ~ 30 μm. Moreover, Lei et al reported a modified co-pressing process to fabricate anode-supported dense and uniform $Ba(Zr_{0.1}Ce_{0.7}Y_{0.2})O_{3-\delta}$ (BZCY) electrolyte films (~20 μm thick).

However, the technique is very important to control thermal expansion coefficients between anodes and electrolytes.

In this study, nano-sized BZCY powders were prepared by different synthesis methods, Pechini and co-precipitation. The physical and electrochemical characteristics were compared, and then used for the electrolytes of the solid oxide fuel cells. Moreover, the anode functional layer was introduced to enhance the interfacial properties between electrodes and electrolytes. We expected that the functional layer with nanocomposite powders of NiO/BZCY and fine BZCY(C) would minimize the mismatch between the electrolyte and the anode supports. The objective of the present work was to examine the total resistance and cell performance of the single cell fabricated by using the two-types BZCY nano-powders and nano-composite anode functional layers.

2. Experimental

2.1. Synthesis

The $Ba(Zr_{0.1}Ce_{0.7}Y_{0.2})O_{3-\delta}$ powder was prepared by using Pechini method (BZCY(P)). Starting materials of $Ba(NO_3)_2$ (Yakuri Pure Chemical Co. 99%), $ZrO(NO_3)_2 \cdot xH_2O$ (Aldrich, 99%), $Ce(NO_3)_3 \cdot 6H_2O$ (Aldrich, 99%) and $Y(NO_3)_3 \cdot 6H_2O$ (Aldrich, 99.8%) were dissolved in distilled water to form an aqueous solution. An appropriate amount of citric acid (Duksan Chemical Co. 99.5%) was added to the solution as a complexing agent, and then the solution was heated and stirred at 60 °C for 2 h. This solution was continuously heated and stirred at 240 °C until it was converted into a pale-yellow ash. The resulting intermediate was calcined at 1000 °C for 3 h to form the perovskite phase.

The BZCY powders (BZCY(C)) were synthesized by the co-precipitation method using a basic solution [19]. Ammonium carbonate ($(NH_4)_2CO_3$, Aldrich, 99%) was used as the co-precipitation medium. Stoichiometric amounts of nitrate salt were dissolved in distilled water, and then dropped into an ammonium carbonate solution with vigorous stirring to complete

precipitation. After that, the suspension was stirred for 2 h and aged for 6 h. Then precipitate was washed several times with distilled water and ethanol. Finally, the precipitate was dried at 100 °C for 24 h and calcined at 1000 °C for 3 h.

The NiO/BZCY-BZCY(C) nanocomposite powder for anode-functional layers was synthesized by a modified Pechini method.[20] The precursors of $Ni(NO_3)_2 \cdot 6H_2O$ (Junsei Chemical Co. 97%) and metal nitrates of Ba, Zr, Ce, and Y were added to distilled water with citric acid, and the precursor solution was heated and stirred at 60 °C for 2 h. The compositions were expected as the same to the $Ba(Zr_{0.1}Ce_{0.7}Y_{0.2})O_{3-\delta}$. Ethylene glycol (Aldrich, 99%) was added to the solution as a polymerization agent. After that, the BZCY(C) powders were added to the polymeric solution as the weight ratio of the NiO to the BZCY is about 5:5. The polymeric solution was burned at 240 °C for 4 h, and a dark grey-colored intermediate was obtained. Lastly, the resulting intermediate was subsequently calcined at 1000 °C for 3h to yield a NiO/BZCY-BZCY(C) nanocomposite powder.

2. 2. Fabrication of the single cell

The anode substrates with a 36-mm diameter were prepared by pressing the NiO-BZCY (6:4 for weight ratio) powder with 10 wt.% carbon blacks (Columbian Chemical, USA) as a pore former at 500 MPa. The substrates were pre-sintered at 1200°C for 3h in air to produce the anode supports. The BZCY electrolytes were coated by dip-coating method. The BZCY slurries were prepared using BZCY(P) and BZCY(C) powders, respectively. The NiO/BZCY-BZCY(C) anode functional layer (AFL) was deposited between the anode support and the electrolyte layer. The anode support coated with the nanocomposite slurry was sintered at 1200 °C for 3 h. Then, the BZCY(C) electrolyte layer was coated on the NiO/BZCY/NiO-BZCY-BZCY(C) AFL. The specific cell configurations are shown in Table 1. All cells coated with each electrolyte were sintered at 1450 °C for 3 h to achieve a dense BZCY electrolyte film. The cathode paste was prepared using $La_{0.6}Sr_{0.4}Co_{0.2}Fe_{0.8}O_3$ (LSCF, Praxair) and

$Ba(Zr_{0.1}Ce_{0.7}Y_{0.2})O_{3-\delta}$. The cathode paste was screen-printed on the anode-supported electrolyte to be a thickness of 20~ 30 μm and an active area of 1.0 cm^2. The final cells were sintered at 1100 °C for 3 h.[21]

2.3. Characterizations and Single cell tests

The crystalline phases of the prepared BZCY and NiO/BZCY-BZCY(C) powders were detected by X-ray diffraction (XRD) spectroscopy (Rigaku, Miniflex). A field emission scanning electron microscope (FE-SEM, LEO SUPRA 55) was used to observe the microstructure, and energy-disperse X-ray spectroscopy (EDX, GENESIS 2000) was used to observe the diffusion of Ni ions from the anode supports to the BZCY electrolyte.

The cell performances were evaluated at various temperatures (600~800 °C) by feeding humidified hydrogen (200 $cm^3\,min^{-1}$) with 3% H_2O to the anode side and air (300 $cm^3\,min^{-1}$) to the cathode side, respectively. The I-V curves were obtained by using a digital multi-meter (Kikusui, KFM2000). The resistances were measured using AC impedance spectroscopy (Autolab, PGSTAT-30) at a frequency range from 0.1 MHz to 0.1 Hz with a signal amplitude of 10 mV.

3. Results and discussion

Figure 1 shows the X-ray diffraction (XRD) patterns of the $Ba(Zr_{0.1}Ce_{0.7}Y_{0.2})O_{3-\delta}$ powders synthesized by Pechini and co-precipitation methods. The XRD patterns of the BZCY powders were assigned to a simple cubic perovskite structure. There were no secondary phases in the BZCY(C) powders (Fig. 1), while the BZCY(P) showed the XRD patterns of some impurities associated with the $BaCO_3$ and CeO_2.[22] This may be due to NO_3 interaction: the rapid heating rate can provide the synthesis condition, $2NH_4NO_3 \rightarrow 2N_2 + O_2 + 4H_2O$, instead of $NH_4NO_3 \rightarrow N_2O + 2H_2O$. In this study, we set the heating temperature to about 5 °C per min, and therefore the second reactions may be predominant, which can lead to the formation of $BaCO_3$ by residual carbons.

Figure 2 shows the SEM images of the BZCY(C) and BZCY(P) powders calcined at 1000 °C for 3 h in air. The BZCY(C) powders were relatively smaller and more uniform than the BZCY(P) powders in a particle size. As shown in Figure 3, the average particle size of the BZCY(C) powders was about 50~ 150 nm, while the BZCY(P) powders had a particle size of about 500~ 900 nm.

Figure 4 shows the pore size distributions and hydrogen permeability of both the BZCY (C) and BZCY (P) electrolytes. The BZCY(P) electrolytes were still porous with 0.189 $m^2 g^{-1}$ of pore area and 9.4771 % of porosity even after sintered at 1450 °C for 3 h. However, the pore sizes were close to zero with negligible total pore area and porosity in the BZCY (C) electrolytes. This indicates that the BZCY(P) electrolytes have a poorer sinterability than the BZCY(C) electrolytes at 1450 °C. The reason for this may be larger particle size of the BZCY (P) than the BZCY (C). To provide further comparison of the sinterability between BZCY(C) and BZCY(P) electrolytes, the hydrogen permeability of the electrolytes was measured at room temperature. The corresponding results are shown in Figure 4. The BZCY(P) electrolyte showed 10^{-6}~10^{-7} mol m^{-2} s^{-1} Pa^{-1} of hydrogen permeability, while the BZCY(C) electrolyte had ~10^{-9} mol m^{-2} s^{-1} Pa^{-1} of hydrogen permeability. It suggests that the co-precipitation method is more suitable to obtain dense impermeable BZCY films.

Figure 5 shows the cross-section of the cells with nickel line scanning by EDX. Figure 5 (a) implies that the nickel ions in the anodes may diffuse into the interface between the cathode and electrolytes. The nickel seems to have penetrated through the grain boundary and the pores of the electrolyte to the cathode layer during the sintering in high temperature [23-26]. The nickel ions in the interfaces between the electrolytes and cathodes may be transformed into NiO with oxygen ions, and interfere the transfer of protons through grain boundaries. On the other hand, there were no traces of Ni ions in the interfaces between the BZCY (C) electrolytes and cathodes. Thus, we selected the BZCY (C) electrolytes and the NiO/BZCY-

BZCY(C) nano-composite AFL was introduced to further enhance the cell performances as shown in Figure 5 (C). It is also expected that the AFL could contribute to minimizing the interfacial resistance and mismatch between the porous anode support and the dense electrolyte in the single cells.[19] All electrolytes were about 25-30 μm, and the AFL was about 10 μm in a thickness.

Figure 6 shows the I-V curves and power densities on the cells with different configurations. As shown in Figure 6 (a), the open circuit voltages (OCVs) of the cell with BZCY (P) electrolytes were 0.99, 1.06, and 0.97 V at 800, 700 and 600 °C, respectively. In addition, the cell performances were also dropped from about 0.22 Wcm^{-2} at 800 °C to 0.07 Wcm^{-2} at 600 °C. These values are quite lower than other literatures.[26-28] The low OCVs and power densities may be caused by gas crossover through the BZCY (P) electrolytes and the Ni ion penetrations into the cathodes as mentioned earlier. The maximum power densities of the cell with the BZCY(C) electrolytes were about 0.4, 0.3, and 0.23 Wcm^{-2} at 800, 700 and 600 °C, respectively, as shown in Figure 6 (b). The improved performance can result from high OCV values with dense electrolytes which may block the Ni penetrations. The cell consisting of the nano-composite AFL and BZCY (C) electrolytes had OCVs of 0.95, 1.02, and 1.08 V, and maximum power densities of 0.8, 0.47, and 0.31 Wcm^{-2} at 800, 700 and 600 °C, respectively (Figure 6 (C)). The BZCY-based cell performance was further increased by introducing the nano-composite anode functional layers. The results confirmed that the AFL improves the electrochemical reaction on the interfaces between the anode and electrolyte by reducing the structural mismatches and the interfacial resistances.

The variation of the area specific resistances (ASRs) of anode-supported cells as determined from the impedance spectra is shown in Figure 7. The ohmic resistances mainly arising from the electrolyte and all contact resistances were obtained from high-frequency intersection with the x-axis. The ohmic and electrode resistances were decreased with the

increase in the operating temperature. In the cell with the BZCY(P) electrolytes, the ohmic resistance was about 0.57 Ω cm^2 at 800 °C. The high resistance is a result of the electrolyte containing high porosity and wide pore areas, which interrupts the conduction of proton along the grain boundary. On the other hand, the cells with BZCY (C) electrolytes and AFL/BZCY (C) electrolytes showed low ohmic resistances of 0.31 and 0.13 Ω cm^2, respectively because of their pore-free electrolytes. The electrode resistances of the cells include the cathode-electrolyte interface resistances and the anode-electrolyte interface resistances. As expected, the increase in the operating temperature resulted in a significant reduction of interfacial resistance. The electrode resistances of the cell with BZCY (P) were larger than that of the cell with BZCY (C) electrolytes at all temperatures. It corresponds well to the results of the cell performances. Particularly, the cell with anode functional layer/BZCY (C) electrolytes showed a much smaller resistance of 0.93 Ω cm^2 at 600 ^oC compared with other two samples. The results suggest that the BZCY electrolytes prepared by co-precipitation were more suitable for low-temperature solid oxide fuel cells, and the introduction of the AFL can improve the cell performances.

4. Conclusions

The dense electrolyte with a porosity of 0.001% was obtained from the BZCY (C) nano-powders, which prevented gas crossover for the BZCY-based single cell. However, the BZCY (P) showed porous electrolytes and secondary phases in the XRD patterns. These had negative impact on the cell performances. The cell performances were higher in the following order of the cells: BZCY (P), BZCY (C), and nano-composite anode functional layer/BZCY (C). The AFL decreased the electrode resistances, which is due to formation of well-connected interfaces. We expect that nano-sized BZCY (C) powders would contribute to enhancements in the SOFC performances, and the nano-composite AFL can be effective in reducing electrode resistances at low-temperatures.

Acknowledgement

This research was supported by Basic Science Research Program through the National Research Foundation of Korea (NRF) funded by the Ministry of Education (NRF-2017R1A6A3A03004416) and (NRF-2015M1A2A2056833).

† These authors contributed equally to this work.

References

[1] N. Q. Minh, Ceramic fuel cells, J. Am. Ceram. Soc. 76 (1993) 563.

[2] Z. P. shao, S.M. Haile, A high-performance cathode for the next generation of solid-oxide fuel cells, Nature 431 (2004) 170.

[3] P. Murray, T. Tsai, S.A. Barnett, A direct-methane fuel cell with a ceria-based anode , Nature 400 (1999), 649.

[4] B.C. H. Steele, Material science and engineering: the enabling technology for the commercialisation of fuel cell systems, J. Mater. Sci. 36 (2001), 1053

[5] B.C. H. Steele, A. Heinzel, Materials for fuel-cell technologies, *Nature* 2001, 414, 345.

[6] Y. Yamazaki, P. Babilo, S.M. Haile, Defect chemistry of yttrium-doped barium zirconate: A thermodynamic analysis of water uptake, Chem. Mater. 20 (2008), 6352–6357

[7] K. Katahira, Y. Kohchi, T. Shimura, H. Iwahara, Protonic conduction in Zr-substituted BaCeO 3, Solid State Ionics 138 (2000), 91.

[8] L. Yang, C. Zuo, S. Wang, Z. Cheng, M. Liu, A Novel Composite Cathode for Low-Temperature SOFCs Based on Oxide Proton Conductors, Adv. Mater. 20 (2008) 3280

[9] L. Yang, S. Wang, K. Blinn, M. Liu, Z. Liu, Z. Cheng, M. Liu, Enhanced sulfur and coking tolerance of a mixed ion conductor for SOFCs: BaZr0. 1Ce0. 7Y0. 2–

xYbxO3–δ, Science, 326 (2009) 126

[10] W. Sun, L. Yan, B. Lin, S. Zhang, W. Liu, High performance proton-conducting solid oxide fuel cells with a stable Sm 0.5 Sr 0.5 Co 3− δ–Ce 0.8 Sm 0.2 O 2− δ composite cathode, J. Power Sources, 195 (2010) 3155

[11] H. Iwahara, Proton conducting ceramics and their applications, Solid State Ionics 86–88 (1996), 9.

[12] T. Norby, Solid-state protonic conductors: principles, properties, progress and prospects, Solid State Ionics 125 (1999), 1.

[13] D.H. Seo, S.S. Park, B.M. Lim, Y.G. Shul, Multicomponent Proton Conducting Ceramics of SiO2–TiO2–ZrO2–P2O5–Bi2O3 for an Intermediate Temperature Fuel Cell, J. Fuel Cell Sci. Technol. 8 (2011), p.011012

[14] K.H. Ryu, S.M. Haile, Chemical stability and proton conductivity of doped BaCeO 3–BaZrO 3 solid solutions, Solid State Ionics 125 (1999), p. 355.

[15] H. Iwahara , Technological challenges in the application of proton conducting ceramic, Solid State Ionics 77 (1995) 289-298

[16] C.D. Zuo, S. Zha, M. Liu, M. Hatano, M. Uchiyama, Ba (Zr0. 1Ce0. 7Y0. 2) O3–δ as an electrolyte for low-temperature solid-oxide fuel cells, Adv. Mater. 18 (2006), pp. 3318–3320.

[17] Z. Zhu, W. Sun, L. Yan, W. Liu, W. Liu, Synthesis and hydrogen permeation of Ni–Ba (Zr 0.1 Ce 0.7 Y 0.2) O 3− δ metal–ceramic asymmetric membranes, Int. J. Hydrogen Energ. 36 (2011) 6337

[18] L. Yang, C. Zuo, M. Liu, High-performance anode-supported Solid Oxide Fuel Cells based on Ba (Zr 0.1 Ce 0.7 Y 0.2) O 3− δ (BZCY) fabricated by a modified co-pressing process, J. Power Sources, 195 (2010) 1845

[19] A.I.Y. Tok, L.H. Luo, F.Y.C. Boey, Carbonate Co-precipitation of Gd 2 O 3-doped

CeO 2 solid solution nano-particles, Materials Science and Engineering A 383 (2004) 229-234.

[20] S.D. Kim, H. Moon, S.H. Hyun, J. Moon, J. Kim, H.W. Lee, Nano-composite materials for high-performance and durability of solid oxide fuel cells, J. Power Sources 163 (2006) 392-397.

[21] L. Yang, Z. Liu, S. Wang, Y.M. Choi, C. Zuo, M. Liu, A mixed proton, oxygen ion, and electron conducting cathode for SOFCs based on oxide proton conductors, J. Power Sources 195 (2010) 471-474.

[22] E. Fabbri, A. D'Epifanio, E.D. Bartolomeo, S. Licoccia, E. Traversa, Tailoring the chemical stability of Ba(Ce0.8−xZrx)Y0.2O3−δ protonic conductors for intermediate temperature solid oxide fuel cells (IT-SOFCs), Solid State Ionics 179 (2008) 558-564.

[23] H.-W. Wang, Inhibition of the formation of barium carbonate by fast heating in the synthesis of BaTiO3 powders via an EDTA gel method, Mater. Chem. Phys., 74 (2002) 1-4

[24] A. M. Myasnikov, M. C. Poon, P. C. Chan, K. L. Ng, M. S. Chan, W. Y. Chan, S. Singla, C. Y. Yuen, On mechanism of nickel diffusion during metal induced lateral crystallization of amorphous silicon , Mater. Res. Soc. 715 (2002) A22.11.1-4.

[25] A.C.S. SABIONI, A.M. HUNTZ, J.N.V. SOUZA, M.D. MARTINS, F. JOMARD, Diffusion of nickel in single-and polycrystalline Cr2O3, Philosophical Magazine 88(2008) 391-405

[26] Y. Guo, R. Ran, Z. Shao, A novel way to improve performance of proton-conducting solid-oxide fuel cells through enhanced chemical interaction of anode components, Int. J. Hydrogen. Energ. 36 (2011) 1683-1691.

[27] Y. Guo, Y. Lin, R. Ran, Z. Shao, Zirconium doping effect on the performance of proton-conducting BaZryCe0.8−yY0.2O3−δ (0.0 ≤ y ≤ 0.8) for fuel cell

applications, J. Power Sources, 193 (2009) 400

[28] C. Zuo, S. Zha, M. Liu, M. Hatano, M. Ba(Zr0.1Ce0.7Y0.2)O3–δ as an Electrolyte for Low-Temperature Solid-Oxide Fuel Cells, Adv. Mater., 18 (2006) 3318

[29] Y. Lin, W. Zhou, J. Sunarso, R. Ran, Z. Shao, Characterization and evaluation of BaCo0.7Fe0.2Nb0.1O3−δ as a cathode for proton-conducting solid oxide fuel cells, International Journal of Hydrogen Energy, 37 (2012) 484

[30]

Figure captions

Fig. 1. X-ray diffraction pattern of the BZCY powders synthesized by Pechini and co-precipitation method.

Fig. 2. SEM images of BZCY powders prepared by (a) Pechini and (b) co-precipitation method

Fig. 3. Particle size distributions of the BZCY powders synthesized by Pechini and co-precipitation method

Fig. 4. Pore size distribution and hydrogen permeability of the BZCY electrolytes synthesized by Pechini and co-precipitation method

Fig. 5. Cross-sectional SEM images and EDX signals for Ni of the single cells after cell test of (a) Cell 1, (b) Cell 2 and (c) Cell 3

Fig. 6. Cell performances of the (a) Cell 1, (b) Cell 2 and (c) Cell 3 under humidified hydrogen atmosphere at 600~800 ^{o}C

Fig. 7. The resistances of the cells determined from the impedance spectra under open-circuit condition at 600~ 800 ^{o}C

Table 1. Cell configurations and porosities of the different single cells

Sample no.	Component of the single cell		Total pore area ($m^2 g^{-1}$)	Porosity of electrolyte (%)
Cell 1	*anode*	NiO-BZCY (P)		
	electrolyte	**BZCY(P)**	0.189	9.4771
	cathode	BZCY-LSCF		
Cell 2	*anode*	NiO-BZCY(C)		
	electrolyte	**BZCY (C)**	0.001	0.5380
	cathode	BZCY-LSCF		
Cell 3	*anode*	NiO-BZCY(C)		
	functional layer	**NiO/BZCY-**		
	electrolyte	**BZCY(C)**	0.001	0.4206
	cathode	**BZCY (C)**		
		BZCY-LSCF		

Figure 1.

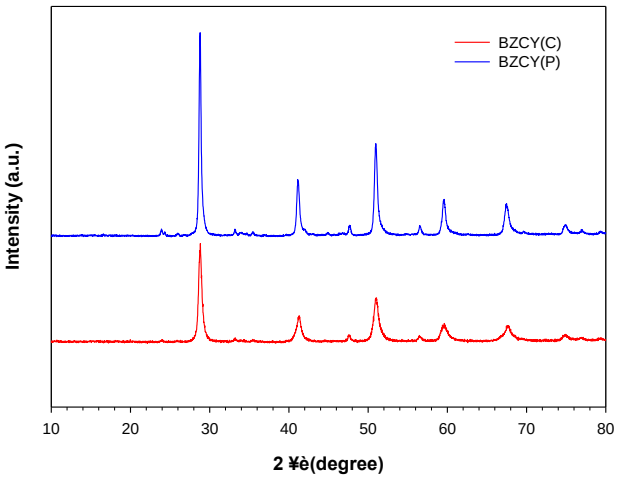

Figure 2.

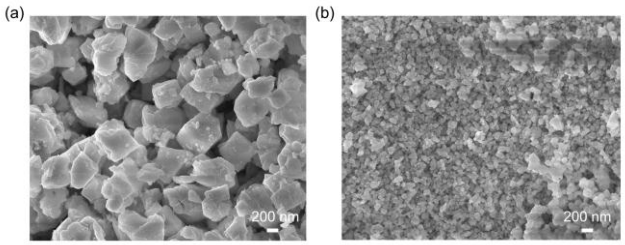

Figure 3.

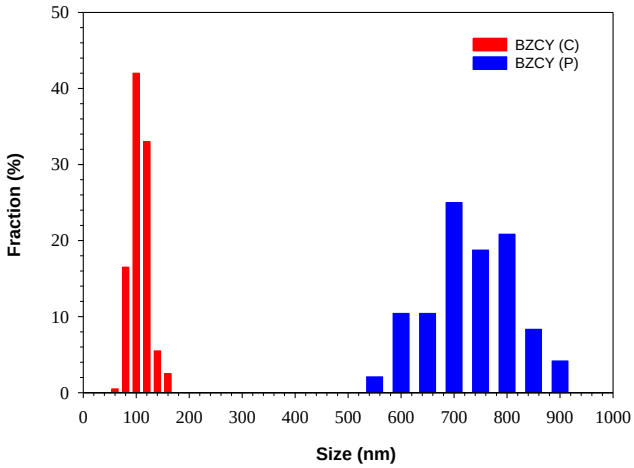

Figure 4.

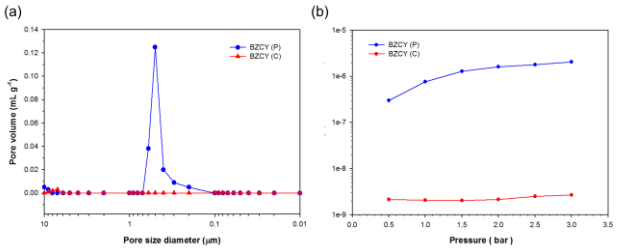

Figure 5.

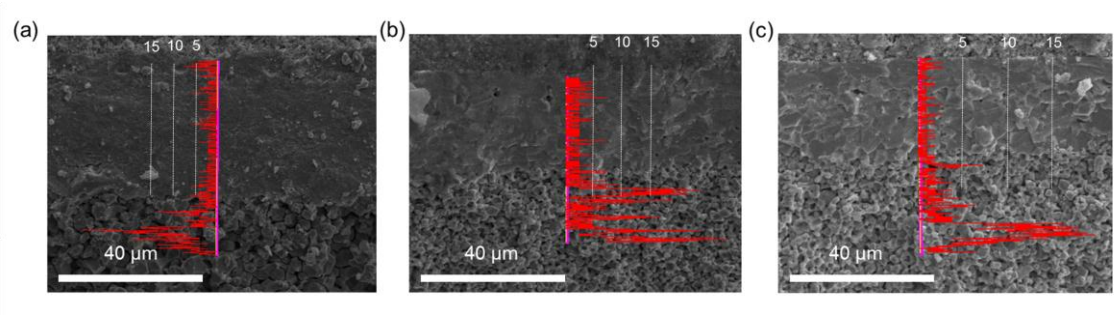

Figure 6.

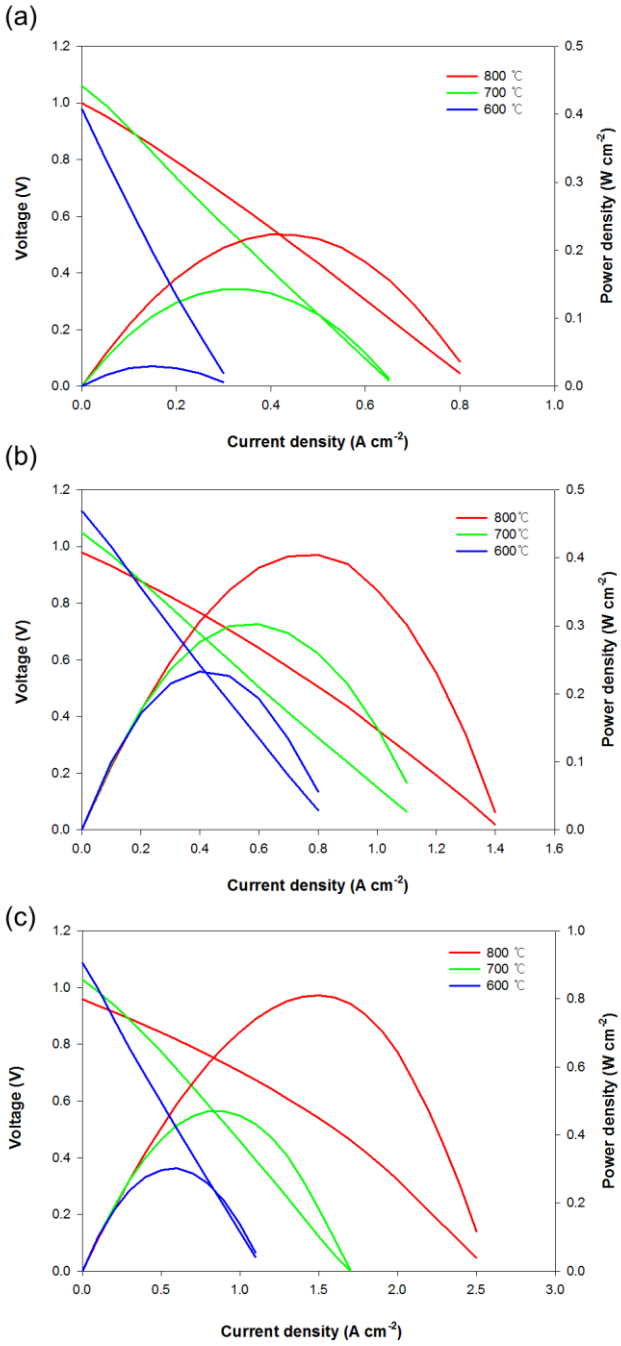
(a)
800 ℃
700 ℃
600 ℃
Voltage (V)
Power density (W cm-2)
Current density (A cm-2)
(b)
800℃
700℃
600℃
Voltage (V)
Power density (W cm-2)
Current density (A cm-2)
(c)
800 ℃
700 ℃
600 ℃
Voltage (V)
Power density (W cm-2)
Current density (A cm-2)

Figure 7.

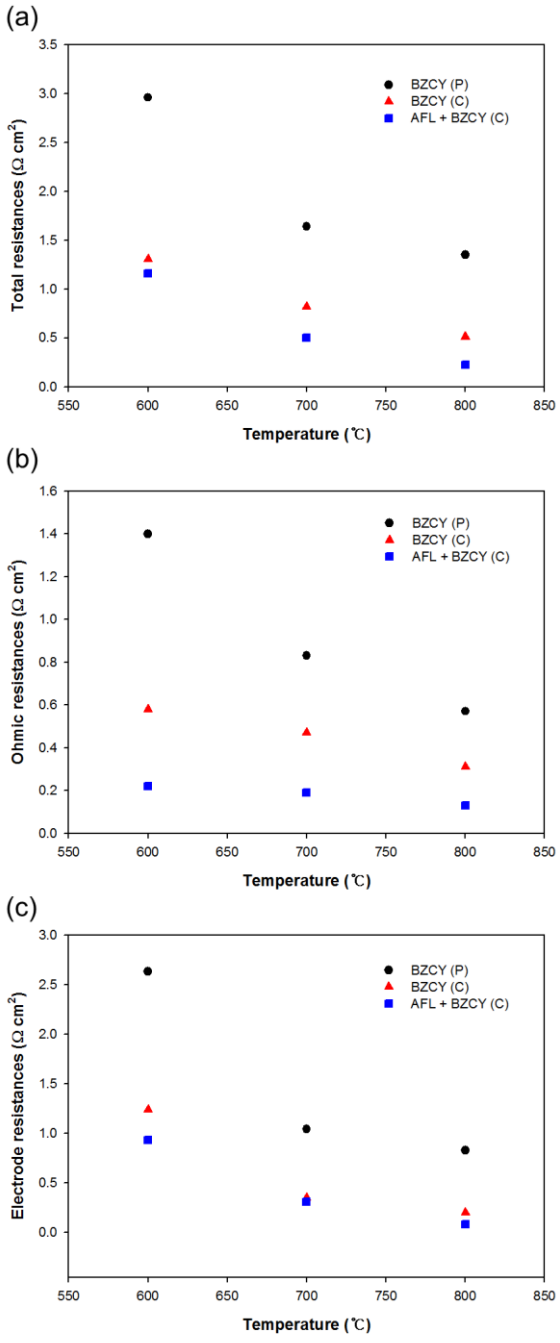
(a)
Total resistances (Ω cm²)
Temperature (℃)
BZCY (P)
BZCY (C)
AFL + BZCY (C)
(b)
Ohmic resistances (Ω cm²)
Temperature (℃)
BZCY (P)
BZCY (C)
AFL + BZCY (C)
(c)
Electrode resistances (Ω cm²)
Temperature (℃)
BZCY (P)
BZCY (C)
AFL + BZCY (C)